Biogeosciences, 11, 2375–2389, 2014
www.biogeosciences.net/11/2375/2014/
doi:10.5194/bg-11-2375-2014

Biogeosciences Open Access

Variability of the transport of anthropogenic CO_2 at the Greenland–Portugal OVIDE section: controlling mechanisms

P. Zunino[1], M. I. Garcia-Ibañez[2], P. Lherminier[1], H. Mercier[3], A. F. Rios[2], and F. F. Pérez[2]

[1]Ifremer, Laboratoire de Physique des Océans, UMR6523 CNRS/Ifremer/IRD/UBO, Ifremer Centre de Brest, CS 10070, Plouzané, France
[2]Instituto de Investigaciones Marinas, IIM-CSIC, 36208 Vigo, Spain
[3]CNRS, Laboratoire de Physique des Océans, UMR6523 CNRS/Ifremer/IRD/UBO, Ifremer Centre de Brest, CS 10070, Plouzané, France

Correspondence to: P. Zunino (pzuninor@ifremer.fr)

Received: 9 September 2013 – Published in Biogeosciences Discuss.: 18 October 2013
Revised: 17 January 2014 – Accepted: 12 March 2014 – Published: 29 April 2014

Abstract. The interannual to decadal variability in the transport of anthropogenic CO_2 (Cant) across the subpolar North Atlantic (SPNA) is investigated, using summer data of the FOUREX and OVIDE high-resolution transoceanic sections, from Greenland to Portugal, occupied six times from 1997 to 2010. The transport of Cant across this section, T_{cant} hereafter, is northward, with a mean value of 254 ± 29 kmol s^{-1} over the 1997–2010 period. We find that T_{cant} undergoes interannual variability, masking any trend different from 0 for this period. In order to understand the mechanisms controlling the variability of T_{cant} across the SPNA, we propose a new method that quantifies the transport of Cant caused by the diapycnal and isopycnal circulation. The diapycnal component yields a large northward transport of Cant (400 ± 29 kmol s^{-1}) that is partially compensated by a southward transport of Cant caused by the isopycnal component (-171 ± 11 kmol s^{-1}), mainly localized in the Irminger Sea. Most importantly, the diapycnal component is found to be the main driver of the variability of T_{cant} across the SPNA. Both the Meridional Overturning Circulation (computed in density coordinates, MOC_σ) and the Cant increase in the water column have an important effect on the variability of the diapycnal component and of T_{cant} itself. Based on this analysis, we propose a simplified estimator for the variability of T_{cant} based on the intensity of the MOC_σ and on the difference of Cant between the upper and lower limb of the MOC_σ (ΔCant). This estimator shows a good consistency with the diapycnal component of T_{cant}, and help to disentangle the effect of the variability of both the circulation and the Cant increase on the T_{cant} variability. We find that ΔCant keeps increasing over the past decade, and it is very likely that the continuous Cant increase in the water masses will cause an increase in T_{cant} across the SPNA at long timescale. Nevertheless, at the timescale analyzed here (1997–2010), the MOC_σ controls the T_{cant} variability, blurring any T_{cant} trend. Extrapolating the observed ΔCant increase rate and considering the predicted slow-down of 25 % of the MOC_σ, T_{cant} across the SPNA is expected to increase by 430 kmol s^{-1} during the 21st century. Consequently, an increase in the storage rate of Cant in the SPNA could be envisaged.

1 Introduction

The ocean acts as an important sink for the CO_2 emitted by human activities. It has stored approximately one third of the total anthropogenic CO_2 (Cant hereafter) emissions since the beginning of the industrial era (Sabine et al., 2004). Cant is uptaken by the air–sea interface and its distribution depends on mixing processes and transport into the ocean interior; this is the reason why Cant generally decreases with increasing depth. The storage of Cant in the deep ocean depends on the ventilation and formation of intermediate and deep waters (Tanhua et al., 2006; Rhein et al., 2007; Steinfeldt et al., 2009).

Among all oceans, the highest rate of Cant storage is found in the North Atlantic, mainly in the subpolar region (Sabine et al., 2004; Khatiwala et al., 2013). An increase in Cant

storage is associated with an increase in the Cant concentration of the water masses. The rate at which the Cant concentration increases in the different water masses depends on both their ages and their positions in the water column. In the subpolar North Atlantic (SPNA hereafter), the upper layers that contain the Subantartic Intermediate Water (SAIW), the Subpolar Mode Water (SPMW) and the North Atlantic Central Water (NACW) present the highest Cant increase trends, changing from average values of 35–40 µmol kg^{-1} in 1991–1993 up to 55 µmol kg^{-1} in 2006 (Pérez et al., 2010). Besides, the production of Labrador Sea Water (LSW) fosters a fast injection of Cant in the intermediate and deep waters, so that this water mass also presents a high trend of Cant increase. Otherwise, the deeper water masses of the Eastern North Atlantic show no significant tendencies in their Cant content between 1991 and 2006 (Pérez et al., 2010).

In the North Atlantic the highest air–sea fluxes of Cant are detected at mid-latitude (Mikaloff Fletcher et al., 2006). Besides, Pérez et al. (2013) have inferred that Cant is the main component of the air–sea CO_2 fluxes at mid-latitude in the North Atlantic, while the natural component is the dominant one in the subpolar region. They also detected a decrease in the storage rate of Cant between 1997 and 2006 in the subpolar region that was related to the reduction in the intensity of the Meridional Overturning Circulation (computed in density coordinates, MOC_σ). Based on those findings, they elucidated the important contribution of the lateral advection of Cant from middle to high latitudes to the Cant storage in the SPNA. The other important element of the Cant storage in the SPNA is the advection of water masses recently ventilated such as the different vintages of Labrador Sea Water. Consequently, how Cant is transported in the SPNA is a crucial issue for understanding how the ocean is storing Cant and for modeling the future role of the ocean damping the atmospheric CO_2 increase caused by mankind.

Nowadays, there is an important international effort in understanding how the ocean uptakes, distributes and stores Cant. On the one hand, there are estimations of CO_2 fluxes computed from sea surface pCO_2 measurements, ocean (model) inversion, atmospheric inversion and/or ocean biogeochemical models. On the other hand, some of these methods also provide an estimation of the transport of Cant (T_{cant} hereafter) in the ocean (see Mikaloff Fletcher et al., 2006; Gruber et al., 2009; Tjiputra et al., 2010), but unfortunately, direct estimations of T_{cant} are not abundant and they are concentrated in the Atlantic Ocean. In the North Atlantic, T_{cant} has been estimated from observational data across 24° N and across a transversal section between 40° N and 60° N. T_{cant} is larger at mid-latitudes than in the northernmost section (see Table 1). There are large differences between the uncertainties given for the T_{cant} estimations in Table 1. These differences are very likely due to the different methods used to compute the volume transport since most of the T_{cant} errors come from the volume transport uncertainties. Comparing the observation-based T_{cant} and T_{cant} estimated by ocean (model) inversions or by biogeochemical models, the observation-based estimations are in general larger than the others (see Table 1), but all of them present large errors. This shows that further improvements are necessary to provide more realistic T_{cant} estimations. To bridge the gap between observations and models, it is necessary to understand better which circulation mechanisms control T_{cant} and its temporal variability. For example, following the results of Pérez et al. (2013), it seems crucial that models reproduce a realistic variability of the Atlantic Meridional Overturning Circulation.

In this work, in order to analyze the T_{cant} variability across the SPNA, data measured between 1997 and 2010 from Greenland to Portugal (FOUREX and OVIDE sections, see Fig. 1) were used. The circulation across this section was described by Lherminier et al. (2007, 2010) and Mercier et al. (2013). Briefly, at gyre scale, the structures intersecting the section are a cyclonic circulation in the Irminger Sea, a cyclonic circulation in the Iceland Basin, the North Atlantic Current (NAC) flowing directly northward east of Eriador Seamount, and lastly, an anticyclonic circulation dominating the West European Basin. Beside this gyre-scale circulation, the MOC_σ is an important feature of the circulation across the OVIDE section. It transports warm, Cant-laden surface water northward in its upper limb, mainly by the NAC. North of the section, waters are transformed in cold waters that are poorer in Cant and flow southwards at depth (the lower limb) mainly close to Greenland, in the Deep Western Boundary Current (DWBC). The limit between the upper and lower limbs of the MOC_σ is defined by σ_1 (potential density referenced to 1000 dbar) equal to 32.14 ± 0.03 kmol m^{-3} (called σ_{MOC}, Mercier et al., 2013).

The MOC_σ has been identified as the element of the circulation mainly driving the heat transport across several transoceanic sections in the North Atlantic; meanwhile, the isopycnal transport has a minor impact (Ganachaud and Wunsch, 2003; Mercier et al., 2013). Recently, Pérez et al. (2013) evaluated the Cant storage rate and the T_{cant} variability across the subpolar gyre, finding a significant impact of the MOC_σ on both of them.

Following Pérez et al. (2013) and using a longer time series, we want to go further. First, we evaluate for the first time the variability of T_{cant} across the SPNA at interannual to decadal timescales. Second, we propose a new method in order to evaluate the effect of the different elements of the ocean circulation on the T_{cant} variability. Third, we propose a simplified estimator for T_{cant} across the SPNA based on the factors chiefly responsible of its variability. Finally, we analyze the influence of the increase in Cant in the ocean in the T_{cant} variability. The paper is organized as follows: data and the main water masses circulating across the OVIDE section are detailed in section 2; T_{cant} computation as well as a new method to clarify the effect of the different component of the circulation on T_{cant} are explained in Sect. 3; the main results

Table 1. Estimations of transport of Cant (T_{cant}) in the North Atlantic from the literature. T_{cant} is often given in Pg C yr^{-1} (1 Pg C yr^{-1} = 2642 kmol s^{-1}).

Reference	Latitude	Time	Method	T_{cant} (kmol s^{-1})
Mikaloff Fletcher et al. (2006)	18° N	1765-1995	Ocean (model) inversion	317 ± 26
Gruber et al. (2009)	24.5° N	1765–1995	Ocean (model) inversion	211
Tjiputra et al. (2010)	24.5° N	1990s–2000s	Biogeochemical model	396 ± 106
Roson et al. (2003)	24.5° N	1992	Observations	634 ± 211
Macdonald et al. (2003)	24.5° N	1992–1998	Observations	502 ± 211
Pérez et al. (2013)	40–60° N	2002–2006 (referred to 2004)	Observations	195 ± 24
Mikaloff Fletcher et al. (2006)	49° N	1765–1995	Ocean (model) inversion	53 ± 26
Tjiputra et al. (2010)	49° N	1990s–2000s	Biogeochemical model	~ 100

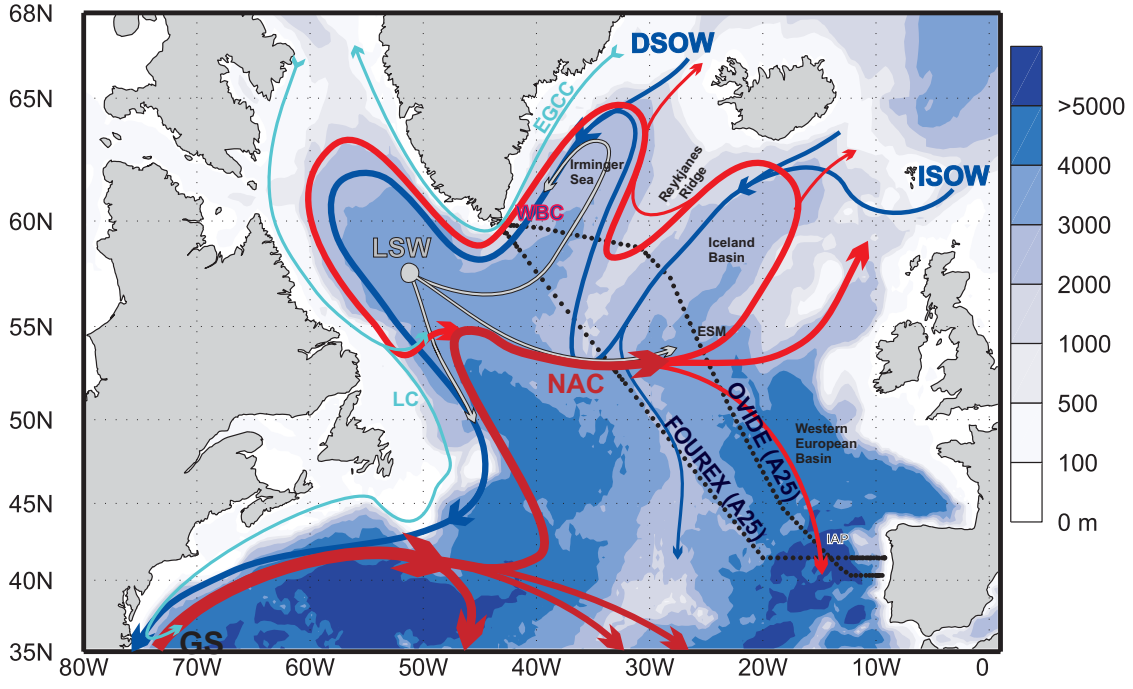

Fig. 1. Schematic circulation in the North Atlantic. The main pathways of warm and salty waters originating from the subtropical Atlantic Ocean are shown in red lines while the deep currents are displayed in dark blue. The cyan lines represent the fresh and cold currents over the shelves (Eastern Greenland Coastal Current (EGCC) and Labrador Current (LC)). The grey lines indicate the spreading of the Labrador Sea Water (LSW). OVIDE and FOUREX sections are represented with dotted lines. The background displays the bathymetry. The other abbreviations are DSOW = Denmark Strait Overflow Water, ISOW = Iceland Scotland Overflow Water, WBC = Western Boundary Current, NAC = North Atlantic Current, GS = Gulf Stream, ESM = Eriador Seamount, and IAP = Iberian Abyssal Plain.

of this work are exposed in Sect. 4; finally, results are discussed in Sect. 5.

2 Data sets

The data used in the study were acquired during the FOUREX and OVIDE cruises (Table 2, Fig. 1), where full-depth hydrographic stations were carried out between Greenland and Portugal. An overview of the instruments and calibrations associated with the physical parameters is presented by Mercier et al. (2013) and summarized hereafter. The CTDO2 measurement accuracies are better than 1 dbar for pressure P, 0.002 °C for temperature T, 0.003 for salinity S and 1 µmol kg^{-1} for dissolved oxygen O_2 (Billant et al., 2004; Branellec and Thierry, 2013). The current velocities perpendicular to the section were estimated by combining the geostrophic currents and the velocities measured by the vessel-mounted acoustic Doppler current profilers in an inverse model using the generalized least squares (Mercier, 1986; Lux et al., 2000). The specificities associated with

Table 2. Hydrographic cruises.

Cruise name	Month/Year	Vessel	Reference
FOUREX 1997	08–09/1997	R/V *Discovery*	Alvarez et al. (2002)
OVIDE 2002	06–07/2002	N/O *Thalassa*	Lherminier et al. (2007)
OVIDE 2004	06–07/2004	N/O *Thalassa*	Lherminier et al. (2010)
OVIDE 2006	05–06/2006	R/V *Maria S. Merian*	Gourcuff et al. (2011)
OVIDE 2008	06–07/2008	N/O *Thalassa*	Mercier et al. (2013)
OVIDE 2010	06–07/2010	N/O *Thalassa*	Mercier et al. (2013)

the OVIDE section are detailed by Lherminier et al. (2007, 2010).

The measurements relative to the CO_2 system were all obtained from bottle samples. The pH was determined with a spectrophotometric method (Clayton and Byrne, 1993), resulting in an accuracy of 0.003 pH units or better. The total alkalinity (A_T) was analyzed with potentiometric titration and determined by single point titration (Pérez and Fraga, 1987; Mintrop et al., 2000), with an accuracy of 4 µmol kg^{-1}. The total inorganic carbon (C_T) was calculated from the pH and total A_T, following the recommendations and guidelines from Velo et al. (2009). Then the concentration of anthropogenic CO_2 (Cant) is determined from C_T, A_T, oxygen, nutrients, T and S, applying the φCt° method (Pérez et al., 2008; Vázquez-Rodríguez et al., 2009). A random propagation of the errors associated with the input variables yielded an overall uncertainty of $\pm$ 5.2 µmol kg^{-1} in the Cant concentration.

The vertical sections of properties (potential temperature (θ), S, Cant) are shown for 2002 and 2010 in Fig. 2. They show the gradient of surface properties from cold, fresh waters in the Irminger Sea to warm, salty and Cant-rich waters toward Portugal. The strongest surface fronts east of the Eriador Seamount (ESM) mark the branches of the North Atlantic Current (NAC, see Lherminier et al, 2010). Note however that the penetration of Cant in the first 1000 m is comparable in the Irminger Sea and in the Iberian Abyssal Plain.

At intermediate depth, the minimum of salinity marks the Labrador Sea Water (LSW) and is observed from the Greenland slope to the Azores–Biscay Rise. Following Yashayaev et al. (2007), we will distinguish two vintages of the LSW: the upper LSW (uLSW), also called LSW_{2000} ($32.32 < \sigma_1 < 32.37$), and the classical LSW (cLSW), also called $LSW_{1987-1994}$ ($32.40 < \sigma_1 < 32.44$). Both classes of LSW are marked by a relative maximum in Cant, due to their recent ventilation in the Labrador Sea, although it is much less clear for the cLSW in 2010, consistent with the fact that this water mass was not ventilated between 1994 and 2008 (Yashayaev and Loder, 2009).

Deep and bottom waters below the LSW have very different properties in the SPNA and in the inter-gyre region. Northwest of the ESM, those waters are rich in overflow waters coming from the Nordic Sea: the Iceland–Scotland Overflow Water (ISOW, below cLSW) and the Denmark Strait Overflow Water (DSOW, below $\sigma_1 = 32.53\,\mathrm{kg\,m^{-3}}$, Tanhua et al., 2005). Southeast of the ESM, the deep and bottom waters are rich in Antarctic Bottom Water (AABW), which has not been in contact with the atmosphere for several decades and presents the lowest concentration of Cant in the whole section. This distribution creates a horizontal gradient of Cant at the bottom, from Cant-free water in the southeast to intermediate Cant concentration in overflow waters in the northwest.

Between 2002 and 2010, the concentration of Cant increased dramatically over the whole section (see Fig. 2), except in the AABW-derived water where Cant concentration is very low. As we will see in the results, this increase has a big impact on the variability of the transport of Cant across the section.

All the trends given in this work were estimated fitting a straight line by means of least squares. Confidence intervals were calculated considering a T student distribution at the 95 % confidence level. The mean values estimated for a period of time are given with the standard error, i.e., $\pm\sigma/\sqrt{N}$, where N is the number of cruises.

3 Method: transport of anthropogenic CO_2 and its decomposition

The transport of any property across the Greenland to Portugal section can be computed as

$$T_{\mathrm{prop}} = \int_{\text{Greenland}}^{\text{Portugal}} \int_{\text{bottom}}^{\text{surface}} v\rho[\mathrm{PROP}]\mathrm{d}x\mathrm{d}z, \quad (1)$$

where v is the velocity orthogonal to the section, ρ is the in situ density and [PROP] is the concentration of any property. Note that x is the horizontal coordinate along the section and z is the vertical coordinate. The error of the transport of any property is calculated taking into account the co-variance matrix of errors of the volume transport obtained from the inverse model; therefore, the errors in the transport of any property come mainly from the volume transport uncertainties.

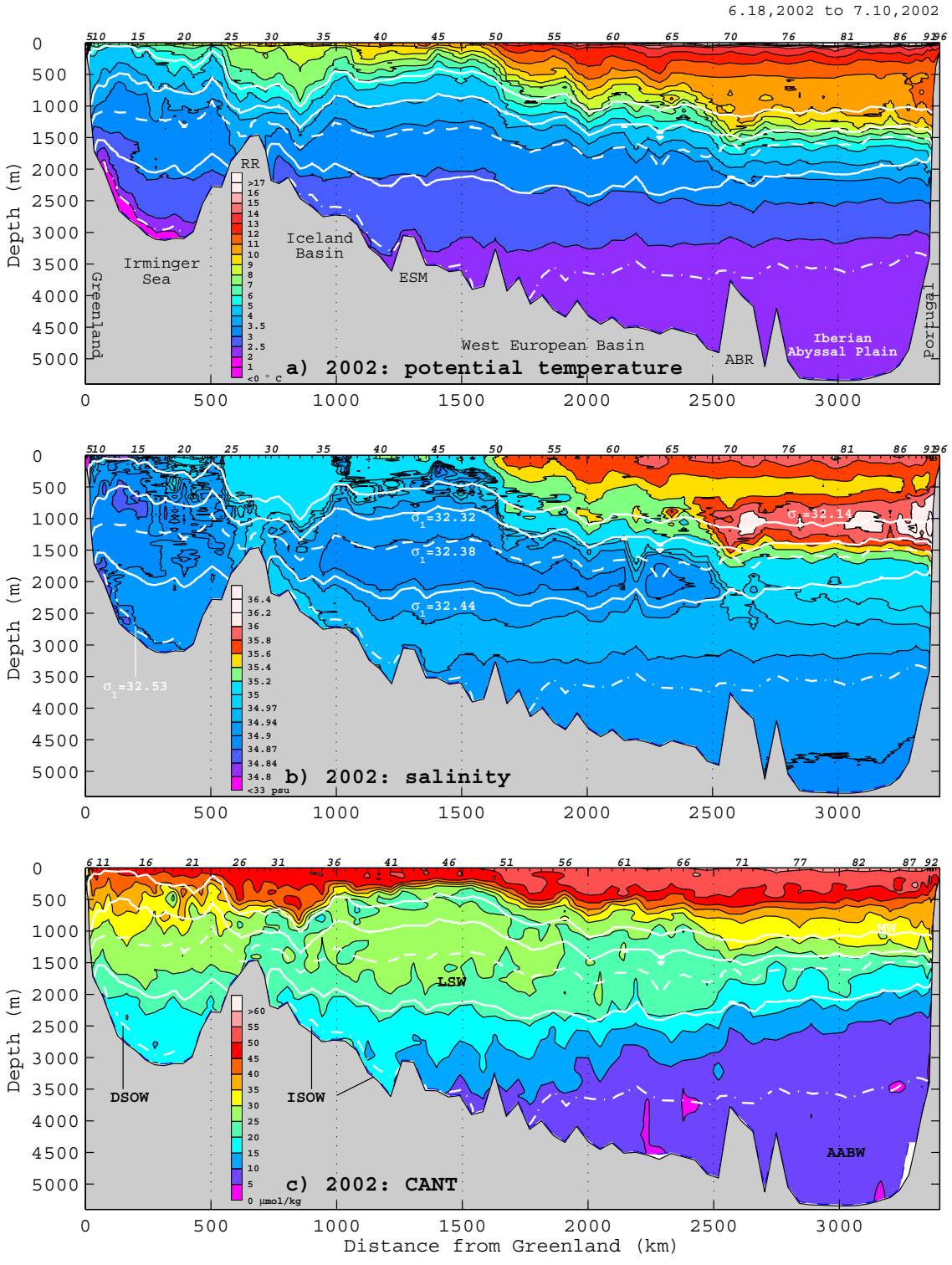

Fig. 2. OVIDE sections of 2002 and 2010 of **(a, d)** potential temperature in °C, **(b, e)** salinity and **(c, f)** anthropogenic CO_2 in µmol kg^{-1}. The depth of the isopycnals referenced in the manuscript are plotted in all the figures; their specific values are indicated in **(b)** and **(e)**. All the water masses cited in the manuscript are localized in the section in **(c)** and **(f)**: DSOW = Demark Strait Overflow Water, ISOW = Iceland Scotland Overflow Water, LSW = Labrador Sea Water, MW = Mediterranean Water, AABW = Antarctic Bottom Water. The other abbreviations in **(a)** and **(d)** are RR = Reykjanes Ridge, ESM = Eriador Sea Mount and ABR = Azores–Biscay Ridge. The numbers at the top of each plot indicate the station numbers corresponding to each survey.

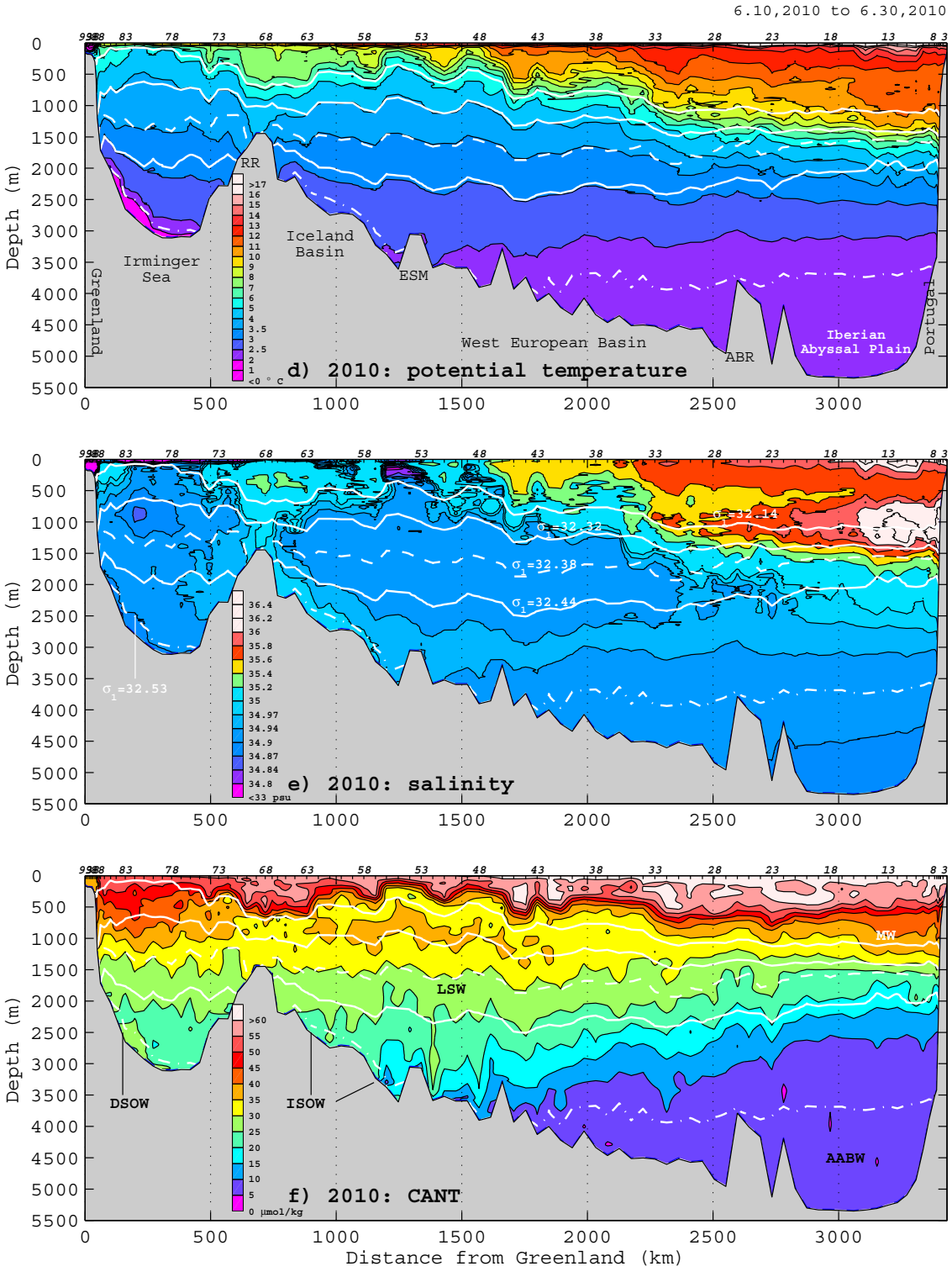

Fig. 2. Continued.

Understanding the processes by which the ocean transports heat, freshwater and Cant is an important issue in climate modeling. In order to evaluate the elements of the circulation that influence the heat transport across transoceanic sections, several authors, for example Böning and Herrman (1994) or Bryden and Imawaki (2002), suggested the decomposition of heat transport into three parts. This methodology has been widely applied for both heat and salt fluxes in the majority of the oceans, but in the case of Cant, it has only been applied by Alvarez et al. (2003). Following the previous authors, for a transoceanic section velocity (V), Cant can be split into

$$V(x,z) = V_0 + \langle v\rangle(z) + v'(x,z) \tag{2}$$

$$\mathrm{Cant}(x,z) = \langle \mathrm{Cant}\rangle(z) + \mathrm{Cant}'(x,z), \tag{3}$$

where $v = V(x,z) - V_0$, V_0 representing the section-averaged velocity corresponding to the net transport across the section. $\langle v\rangle(z)$ is the mean vertical profile of velocity anomalies and $\langle \mathrm{Cant}\rangle(z)$ is the mean vertical profile of Cant. $v'(x,z)$ and $\mathrm{Cant}'(x,z)$ are the deviations from the corresponding mean vertical profiles. In the same way the transport of Cant (T_{cant}, Eq. 1) can be decomposed into three components (Eq. 4) where the overbar denotes the area integration:

$$T_{\mathrm{cant}} = \rho V_0 \overline{\langle \mathrm{Cant}\rangle(z)} + \rho \overline{\langle v\rangle(z)\,\langle \mathrm{Cant}\rangle(z)} + \rho \overline{v'(x,z)\mathrm{Cant}'(x,z)} \tag{4}$$

Alvarez et al. (2003) carried out the decomposition of T_{cant} across the FOUREX section (see Fig. 1) using pressure as a vertical coordinate, the same way as heat and salt transport decompositions are usually done. Because of the strong horizontal density gradient and the general circulation patterns across the section, we think that it is preferable to do the decomposition in a density coordinate ($z = \sigma_1$). Indeed, along the OVIDE section, the upper and lower branches of the Meridional Overturning Circulation, namely, the northward North Atlantic Current (NAC) and the southward Western Boundary Current (WBC), respectively, overlap in the depth coordinate, while they have nearly distinct density properties. Therefore, when the Meridional Overturning Circulation is computed in a pressure coordinate, its intensity is underestimated (Lherminier et al. 2010; Mercier et al., 2013). Thus, we think that T_{cant} computation and decomposition should be done in a density coordinate.

It is the very first time that the T_{cant} decomposition exposed in Eq. (4) is computed in a density coordinate. Regarding the order of the different terms, Eq. (4) can be written as

$$T_{\mathrm{cant}} = T_{\mathrm{cant}}^{\mathrm{net}} + T_{\mathrm{cant}}^{\mathrm{diap}} + T_{\mathrm{cant}}^{\mathrm{isop}}, \tag{5}$$

where

$$T_{\mathrm{Cant}}^{\mathrm{net}} = \rho V_0 \overline{\langle \mathrm{Cant}\rangle(\sigma_1)} \tag{6}$$

$$T_{\mathrm{Cant}}^{\mathrm{diap}} = \rho \overline{\langle v\rangle(\sigma_1)\,\langle \mathrm{Cant}\rangle(\sigma_1)} \tag{7}$$

$$T_{\mathrm{Cant}}^{\mathrm{isop}} = \rho \overline{v'(x,\sigma_1)\mathrm{Cant}'(x,\sigma_1)}. \tag{8}$$

Therefore, $T_{\mathrm{Cant}}^{\mathrm{net}}$ is the net transport of Cant across the section related to a northward transport of about 1 Sv associated with the Arctic mass balance (Lherminier et al., 2007). $T_{\mathrm{Cant}}^{\mathrm{diap}}$ is the transport of Cant linked to the diapycnal circulation that accounts for the light to dense water mass conversion north of the section (Grist et al., 2009) related to the overturning circulation. Lastly, $T_{\mathrm{Cant}}^{\mathrm{isop}}$ quantifies the transport of Cant due to the isopycnal circulation, i.e., the integration of how Cant and transport co-vary in each layer. This term is usually called horizontal circulation when the decomposition is done in pressure coordinates (e.g., Bonning and Herrmann, 1992); however, in our case, it is not the horizontal circulation, since isopycnals present important slopes all along the section (see Fig. 2).

Using the same methodology as Alvarez et al. (2003) but changing the vertical coordinate from pressure to density levels, we expect to find a larger contribution of the overturning component to the total T_{cant} in the same way that the Meridional Overturning Circulation intensity across the section increases when it is computed in density space.

4 Results

4.1 Transport of anthropogenic CO_2 across the Greenland–Portugal section

The transport of Cant (T_{cant}) across the Greenland–Portugal section from 1997 to 2010 is shown in Fig. 3 (black line). The mean value for the whole period is $254 \pm 29\,\mathrm{kmol\,s^{-1}}$. The standard deviation is $71\,\mathrm{kmol\,s^{-1}}$ (while the errors in each estimate average to $48\,\mathrm{kmol\,s^{-1}}$). Note that a positive T_{cant} value means a northward transport of Cant while a negative value points to a southward transport. At the beginning of the period, in 1997, T_{cant} was $289 \pm 32\,\mathrm{kmol\,s^{-1}}$. This value is far off the one estimated by Alvarez et al. (2003, $116 \pm 126\,\mathrm{kmol\,s^{-1}}$). Because both results correspond to the same data, the difference between them comes from the methodology: on the one hand because the constrains considered for computing the volume transport across the section in Alvarez et al. (2003) and in the present work are different (Lherminier et al., 2007); on the other hand because they did not use the $\varphi\mathrm{Ct}^{\circ}$ approximation for calculating Cant. Later, Pérez et al (2013) computed T_{cant} across the OVIDE section between 2002 and 2006; their mean value for that period is $195 \pm 24\,\mathrm{kmol\,s^{-1}}$. For the same period, we obtain a mean value of $208 \pm 40\,\mathrm{kmol\,s^{-1}}$, a compatible result considering the error bars.

The evolution of T_{cant} between 1997 and 2010 (black line in Fig. 3) presents an interannual variability, with a decrease from 1997 to the mid-2000s (see the mean value

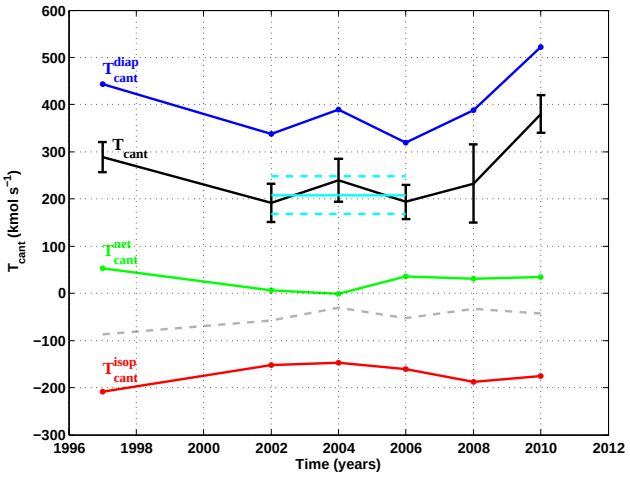

Fig. 3. T_{cant} (black) and its components (blue, red and green) across the OVIDE section as a function of time. The dashed grey line is the transport of Cant due to the Ekman transport; this component is dispatched between the other three components. The cyan lines are the mean value (2002–2006) and the error bars of T_{cant} representative of the mid-2000s.

for 2002–2006 displayed in cyan in Fig. 3) and a recovery hereafter. Note that this T_{cant} recovery and the significant highest value in 2010 ($380 \pm 64\,\mathrm{kmol\,s^{-1}}$) have never been published before. The trend for the whole period of time is $4.0 \pm 15.5\,\mathrm{kmol\,s^{-1}\,yr^{-1}}$. This result is statistically not different from 0 since the interannual variability blurs the longer timescale variability, at least over this 14-year period of time.

4.2 Decomposition of the transport of anthropogenic CO_2 across the Greenland–Portugal section

The evolution of each of the diapycnal ($T_{\mathrm{cant}}^{\mathrm{diap}}$), isopycnal ($T_{\mathrm{cant}}^{\mathrm{isop}}$) and net ($T_{\mathrm{cant}}^{\mathrm{net}}$) transports of Cant are also displayed in Fig. 3. The sum of these three components is exactly the total Cant flowing across the OVIDE section. The 1997–2010 mean values of $T_{\mathrm{cant}}^{\mathrm{diap}}$, $T_{\mathrm{cant}}^{\mathrm{isop}}$ and $T_{\mathrm{cant}}^{\mathrm{net}}$ are $400 \pm 29\,\mathrm{kmol\,s^{-1}}$, $-171 \pm 11\,\mathrm{kmol\,s^{-1}}$ and $26 \pm 9\,\mathrm{kmol\,s^{-1}}$, respectively. For all the years, $T_{\mathrm{cant}}^{\mathrm{diap}}$ is larger than T_{cant}; meanwhile, $T_{\mathrm{cant}}^{\mathrm{isop}}$ is always negative. Finally, the net transport is the smallest contribution to T_{cant} since the net transport of volume across the section is very low, less than 1 Sv, and because the section average of Cant is around $26\,\mu\mathrm{mol\,kg^{-1}}$.

By definition, $T_{\mathrm{cant}}^{\mathrm{isop}}$ is the transport of Cant along isopycnals. It is the area integration of the co-variance of the anomalies of volume transport and Cant at each station and density level across the section; see Eq. (8). We observe that $T_{\mathrm{cant}}^{\mathrm{isop}}$ shows a non-negligible southward transport of Cant across the OVIDE section. The result contrasts with the isopycnal transport of heat (Mercier et al., 2013) that has a minor contribution to the total heat flux in the North Atlantic (Ganachaud and Wunsch, 2003). In the following, we analyze the spatial distribution of $T_{\mathrm{cant}}^{\mathrm{isop}}$ to understand the origin of its southward resultant. Figure 4a displays the mean value of $T_{\mathrm{cant}}^{\mathrm{isop}}$ over 1997–2010, accumulated from Greenland to Portugal and from the bottom to each density level. For water denser than $32.14\,\mathrm{kg\,m^{-3}}$ the accumulated $T_{\mathrm{cant}}^{\mathrm{isop}}$ is $-150\,\mathrm{kmol\,s^{-1}}$, which is the 87 % of the total ($-171\,\mathrm{kmol\,s^{-1}}$). It shows that, for the whole section, the transport of Cant along isopycnals occurs mainly in the dense waters. To locate the main region contributing to $T_{\mathrm{cant}}^{\mathrm{isop}}$, the latter is vertically integrated and horizontally accumulated from Greenland to each station along the section (Fig. 4b). The maximum negative value is reached approximately 200 km from Greenland, exactly where the maximum negative value of volume transport is found (Fig. 4c). From that point eastward, a northward transport of Cant caused by the recirculation in the Irminger Sea diminished the total southward $T_{\mathrm{cant}}^{\mathrm{isop}}$ in this basin (Fig. 4b). In the intermediate and deep waters (deeper than σ_1 equal to $32.14\,\mathrm{kg\,m^{-3}}$) east of Reykjanes Ridge, anomalies of Cant in isopycnal layers are quite small, resulting in a weak contribution to $T_{\mathrm{cant}}^{\mathrm{isop}}$ (Fig. 4b). Instead, taking into account the whole water column, there is a southward $T_{\mathrm{cant}}^{\mathrm{isop}}$ in the Western European Basin (WEB, Fig. 4b) mainly explained by a northward advection (Fig. 4c) of a negative anomaly of Cant in the intermediate layers. Indeed, the shallow isopycnal layers in the Irminger Sea are richer in Cant than the same layers found deeper in the Western European Basin (WEB) and the Iberian Abyssal Plain (IAP; see Fig. 2). We can then conclude that southward transport of Cant associated with the isopycnal component mainly occurs in the Irminger Sea. In order to identify the water masses mainly responsible for this transport, the transport of Cant associated with the isopycnal component is horizontally but not vertically integrated (Fig. 4d). Two different ranges of densities are identified as the major contributions to $T_{\mathrm{cant}}^{\mathrm{isop}}$; the lower lobe ($32.48 < \sigma_1 < 32.55\,\mathrm{kg\,m^{-3}}$) corresponds to the overflow waters (DSOW and ISOW), while the upper lobe corresponds to intermediate and surface waters of the Irminger Sea (note the shallow position of $\sigma_1 = 32.14\,\mathrm{kg\,m^{-3}}$ in the Irminger Sea, Fig. 2). In this basin, the waters corresponding to the density range of both lobes contain high concentrations of Cant (see Fig. 2) due to their recent formation and/or ventilation. To summarize, the southward resultant of $T_{\mathrm{cant}}^{\mathrm{isop}}$ is mainly localized in the Irminger Sea where the southward transport of Cant caused by the Western Boundary Current (WBC) is partially compensated by the northward transport caused by the inner recirculation in this basin. Concerning water masses, only LSW has a minor contribution to $T_{\mathrm{cant}}^{\mathrm{isop}}$; it will be discussed further in Sect. 5.

The transport of Cant across isopycnals, that is $T_{\mathrm{cant}}^{\mathrm{diap}}$, is decomposed in terms of mean profiles of anomalies of volume transport (Fig. 5a) and Cant concentration (Fig. 5b) computed in isopycnal layers (with a resolution of $0.01\,\mathrm{kg\,m^{-3}}$);

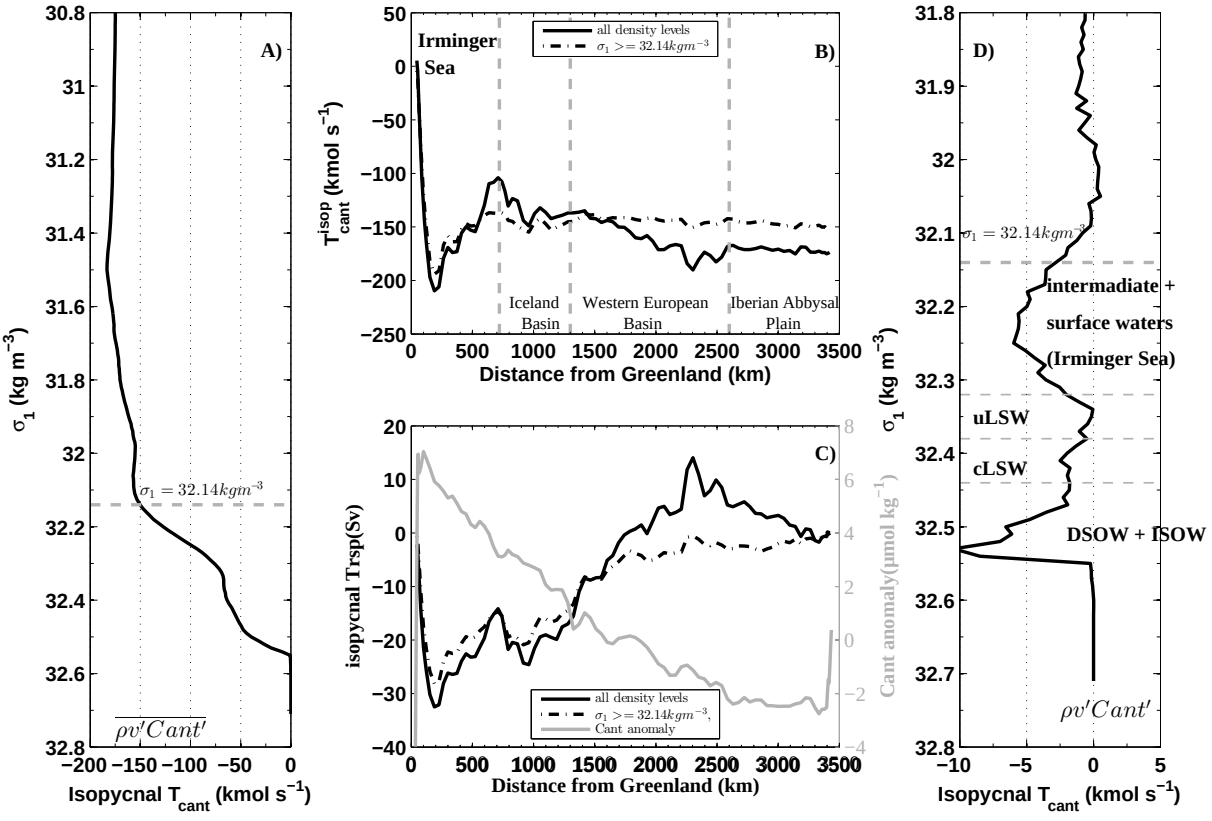

Fig. 4. Transport of Cant caused by the isopycnal component ($T^{\text{isop}}_{\text{cant}}$) averaged over time. **(A)** $T^{\text{isop}}_{\text{cant}}$ accumulated from the bottom to each specific density level. **(B)** $T^{\text{isop}}_{\text{cant}}$ horizontally accumulated from Greenland to each station along the section, and vertically integrated for the whole column of water (continuous lines) and for waters denser than 32.14 kg m^{-3} (dashed lines). **(C)** On the left axis: isopycnal volume transport accumulated from Greenland to each station, and vertically integrated for the whole column of water (continuous black line) and for waters denser than 32.14 kg m^{-3} (dashed black lines). On the right axis, in grey, mean value of Cant anomalies vertically averaged all along the section. **(D)** $T^{\text{isop}}_{\text{cant}}$ horizontally but not vertically integrated (see Fig. 1 for the abbreviations). Note that in plots **(A)** and **(D)**, the vertical axes do not have the same scales.

see Eq. (7). The upper and lower MOC$_\sigma$ limbs can be identified in Fig. 5a, with northward (southward) volume transports above (below) σ_{MOC}. The vertical profile of Cant concentration averaged in density layers is displayed in Fig. 5b; as expected, we observe a decrease in Cant with increasing depth. The profile of transport of Cant (Fig. 5c) follows perfectly the vertical profile of volume transport. The vertical integration of the diapycnal component of the volume transport (Fig. 5a) is equal to 0 Sv. However, because the Cant concentration is larger in the upper limb of the MOC$_\sigma$ than in the lower one (see Fig. 5b), $T^{\text{diap}}_{\text{cant}}$ results in a strong positive value once vertically integrated (see Fig. 3).

The Ekman transport has been estimated separately from wind stress data averaged over the months of the cruises (see Mercier et al., 2013) and equally distributed in the first 30 m. After that, it has been added to the absolute geostrophic velocity across the section and analyzed together. It has not been considered as the fourth element of the circulation because it is dispatched between the diapycnal, isopycnal and net transport. Nevertheless, it is worth mentioning that the Ekman transport causes a southward transport of Cant (see the dashed grey line in Fig. 3), whose mean value is -50 ± 8 kmol s^{-1} and the standard deviation is 21 kmol s^{-1}.

4.3 Variability of the transport of Cant

In this part of the paper, the T_{cant} variability across the OVIDE section is analyzed. We expect that changes in both the circulation and the Cant concentration of water masses have a certain influence on the T_{cant} variability. In the previous section we separated T_{cant} caused by three different elements of the ocean circulation. In this section we are going to evaluate which elements of the circulation have a major influence on the T_{cant} variability and whether the Cant increase in the water masses affects the T_{cant} variability.

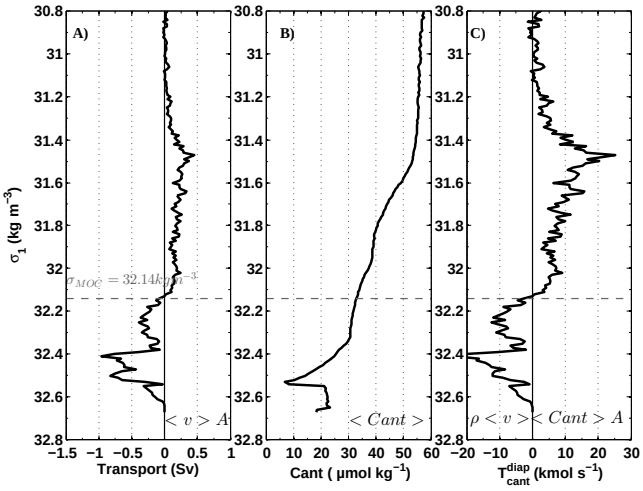

Fig. 5. T^{diap}_{cant} and the different elements by which it was computed (see Eq. 7). **(A)** Profile of anomalies of volume transport integrated into density (σ_1) layers with a 0.01 kg m^{-3} resolution. **(B)** Mean profile of Cant averaged at each density layer. **(C)** T^{diap}_{cant} profile. All the data represented in this figure are the averages of the six surveys analyzed in this work. In the formulation, A means the area of each density layer along the section and replaces the overbar given in Eq. (7), since there is no vertical integration in the data displayed there.

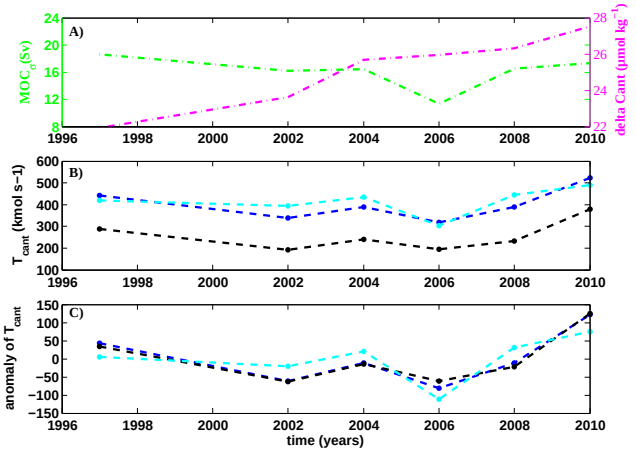

Fig. 6. (A) Time evolution of the intensity of the MOC$_\sigma$ (in green) and the difference in Cant between the upper and lower limbs of the MOC$_\sigma$ (in pink). **(B)** Time evolution of T_{cant} (black line), T^{diap}_{cant} (blue line) and T_{cant} computed by the estimator (T°_{cant}, cyan line). **(C)** Time evolution of anomalies of T_{cant} (black line), T^{diap}_{cant} (blue line), T°_{cant} (cyan line), the anomalies in relation to the mean value computed over 1997–2010.

4.3.1 Variability of the components of T_{cant}

It is observed that the variability of T_{cant} and T^{diap}_{cant} (the black and blue lines in Fig. 3) is very well correlated ($r = 0.99$, p value $= 0.0002$). By contrast, T^{isop}_{cant} presents a small variability that is not correlated with T_{cant} ($r = -0.44$, p value $= 0.38$), and the same is true for T^{net}_{cant} ($r = 0.40$, p value $= 0.43$). From this we can say that the diapycnal component mainly drives the variability of T_{cant}.

In terms of volume transport, the diapycnal component is directly related to the MOC$_\sigma$. Perez et al. (2013) suggested that the weakening of the lateral advection of Cant between 1997 and 2006, caused by the slow-down of the MOC$_\sigma$, is responsible for the decrease in the Cant storage rate during that period. However, during the period of time studied in this work (1997–2010), the MOC$_\sigma$ intensity (Fig. 6a) is correlated neither with T_{cant} ($r = 0.58$, p value $= 0.23$) nor with T^{diap}_{cant} ($r = 0.68$, p value $= 0.13$). These results suggest that, although the diapycnal circulation is related to the MOC$_\sigma$, in the case of T_{cant} there is another factor acting on the T^{diap}_{cant} variability. It is very likely that the Cant concentration change is the other factor controlling the variability of T^{diap}_{cant}, and thus the variability of T_{cant}.

4.3.2 A simplified estimator for the variability of the transport of Cant

The overturning circulation has been identified as the component of the circulation mainly driving the heat flux variability across the subpolar gyre (Mercier et al., 2013). After defining the MOC$_\sigma$ as the maximum of the transport streamfunction computed in density coordinates, these authors approximated the heat transport variability across the OVIDE section, taking into account the temperature difference between the upper limb and the lower limb of the MOC$_\sigma$ and the intensity of the MOC$_\sigma$. This method applied to T_{cant} could help us to clarify the effect of both circulation changes and Cant increase on the T_{cant} variability. Therefore we propose the following estimator:

$$T^{\circ}_{cant} = \Delta\text{Cant} \cdot \rho \cdot \text{MOC}_\sigma \quad (9)$$

where ΔCant is the difference between the mean value of Cant in the upper and lower limbs of the MOC$_\sigma$, ρ is the in situ density and MOC$_\sigma$ is the intensity of the Meridional Overturning Circulation computed in density coordinates (Mercier et al., 2013). The time evolution of MOC$_\sigma$ and ΔCant is shown in Fig. 6a.

We expect this estimator T°_{cant} to be a good approximation of T^{diap}_{cant} because it takes into account the diapycnal circulation via the MOC$_\sigma$ intensity and not the isopycnal component of the circulation. Furthermore, by using the difference in Cant concentration between both limbs of the MOC$_\sigma$, we take into account the Cant increase in waters flowing through the OVIDE section that we expect to have an important role

in the T_{cant}^{diap} variability. As a matter of fact, the estimator T_{cant}° is quite similar to T_{cant}^{diap} (blue and cyan lines in Fig. 6b) and they are well correlated ($r = 0.82$, p value = 0.04).

To compare their variability, the anomalies of T_{cant}, T_{cant}^{diap}, and T_{cant}° time series are plotted in Fig. 6c. Although we see by eye similar patterns between T_{cant} and T_{cant}° anomalies, the correlation ($r = 0.75$, p value = 0.09) is not as good as between T_{cant}^{diap} and T_{cant}° since the estimator does not consider the isopycnal contribution.

In conclusion, T_{cant} cannot be totally inferred from the proposed estimator (T_{cant}°) since the isopycnal component has a non-negligible contribution, but it is a good estimation of T_{cant}^{diap}. As T_{cant}^{diap} mainly drives the T_{cant} variability across the OVIDE section, T_{cant}° is, at least, a fairly good indicator of the variability of T_{cant} across the section. Moreover, it will help us to disentangle the relative contribution of the circulation and the Cant increase in the variability of T_{cant}.

4.3.3 The effect of Cant concentration changes on the variability of the transport of Cant

In the OVIDE section during the period 1997–2010, the section-average Cant has increased at a rate of $0.29 \pm 0.21\,\mu mol\,kg^{-1}\,yr^{-1}$, which means an increase of $4\,\mu mol\,kg^{-1}$ between 1997 and 2010. The Cant increase in the upper limb of the MOC_σ, which imports Cant into the subpolar region, is larger than the increase in the lower limb, which exports Cant from the subpolar region: $0.63 \pm 0.27\,\mu mol\,kg^{-1}\,yr^{-1}$ and $0.20 \pm 0.25\,\mu mol\,kg^{-1}\,yr^{-1}$, respectively; see Fig. 7.

In the previous section we presented an estimator, T_{cant}°, which is a good indicator of the T_{cant} variability across the OVIDE section. Using this estimator, if a steady circulation hypothesis is considered (MOC_σ constant, e.g., 16 Sv), T_{cant}° increases at a rate of $7.0 \pm 1.6\,kmol\,s^{-1}\,yr^{-1}$. It means that the Cant increase in the ocean waters yields an increase in the northward transport of Cant across the OVIDE section. However, the overturning circulation has an important role in the T_{cant} variability, and it introduces a larger variability than the Cant increase at the interannual timescale. This is why the "real" trend estimated for T_{cant} for the period 1997–2010 is positive but not statistically different from 0.

To assess the relative role of the Cant concentration and circulation in T_{cant} and to compare it with the analysis of Pérez et al. (2013), we choose to study the period between 1997 and 2006. During that period, the MOC_σ intensity across the OVIDE section decreased (Mercier et al., 2013) at a rate of $0.68 \pm 0.65\,Sv\,yr^{-1}$. Simultaneously, T_{cant} decreased at a rate of $9.3 \pm 11.7\,kmol\,s^{-1}\,yr^{-1}$, while the Cant concentration increased at a rate of $0.48 \pm 0.56\,\mu mol\,kg^{-1}\,yr^{-1}$ and $0.01 \pm 0.42\,\mu mol\,kg^{-1}\,yr^{-1}$ in the upper and lower limbs of the MOC_σ, respectively. All these trends are not statistically different from 0, likely due to the low number of data, only 4, but they give insights that

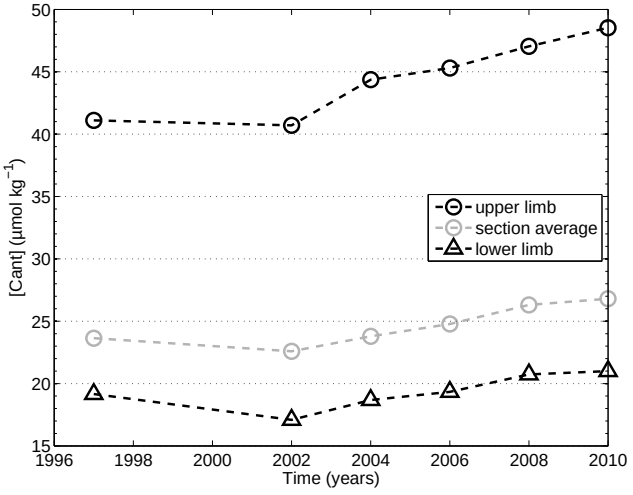

Fig. 7. Time evolution of Cant concentrations: upper limb of the MOC_σ (empty black circles), section average value (empty grey circles), and lower limb of the MOC_σ (empty black triangles).

Cant increased in the upper limb of the MOC_σ; meanwhile it hardly changed in the lower limb. Taking into account these results we conclude that, in the period between 1997 and 2006, the MOC_σ decrease prevailed on the T_{cant} variability. Indeed, using the proposed estimator (T_{cant}°), if a steady circulation was considered, T_{cant} would increase at a rate of $7.8 \pm 3.2\,kmol\,s^{-1}\,yr^{-1}$ during the period 1997–2006. However, if Cant is maintained constant between 1997 and 2006, T_{cant} would decrease at a rate of $15.3 \pm 14.6\,kmol\,s^{-1}\,yr^{-1}$, that is, the slow-down of the MOC_σ would cause a decrease in T_{cant} statistically different from 0.

Over the whole studied period, 1997–2010, we found that the trends in T_{cant} and T_{cant}° are not significant. In the hypothetical case of a steady circulation, T_{cant}° increases at a rate of $7.0 \pm 1.6\,kmol\,s^{-1}\,yr^{-1}$ since ΔCant is continuously increasing. Conversely, if ΔCant remains constant, T_{cant}° variability follows the MOC_σ variability with no trend.

All these results suggest that, at interannual to decadal timescales, the variability of the MOC_σ mainly drives the T_{cant} variability across the OVIDE section. Nonetheless, the Cant increase also causes a long-term increase in T_{cant} that, at the timescale analyzed here, is blurred by the interannual variability caused by the MOC_σ variability.

5 Discussion and conclusions

The continuous increase in CO_2 concentration in the atmosphere due to human activities is softened by the oceanic CO_2 uptake. The question is how long the ocean will act as a sink for this greenhouse gas. Therefore, it is really important to quantify and understand the mechanisms acting in its transport and storage in the oceans. It is well known that the North Atlantic presents the highest storage rate of Cant of

the global oceans, mainly in the SPNA (Sabine et al., 2004). Recently, it has been demonstrated that the lateral advection provides the main supply of Cant to the SPNA (Pérez et al., 2013). In the last decade, the estimations of T_{cant} by observational data and models have yielded quite different results: models tend to show lower values than data (Table 1). In this work we have focused in the physical aspect of the transport of Cant in order to understand the mechanisms driving T_{cant} across the SPNA and to describe for the first time its interannual to decadal variability.

In agreement with previous works (Alvarez et al., 2003 and Pérez et al., 2013), we obtained a northward T_{cant} across the section. The mean value for the period 1997–2010 is $254 \pm 29\,\text{kmol}\,\text{s}^{-1}$; its standard deviation is $71\,\text{kmol}\,\text{s}^{-1}$. No significant long-term changes have been identified during this period, due to the clear decrease between 1997 and the mid-2000s (cyan values in Fig. 3) and the recover thereafter. We have observed that the initial decrease was due to the slow-down of the MOC_σ and that the increase that follows was mainly due to the increase in the Cant concentration in the ocean waters.

Splitting T_{cant} into its different components, we have observed that the isopycnal component causes a non-negligible southward transport (see Fig. 3), mainly localized in the Irminger Sea (see Fig. 4). It contrasts with the heat fluxes across the North Atlantic Ocean, for which the isopycnal component has a minor contribution to the total heat flux (Ganachaud and Wunsch, 2003); across the OVIDE section specifically, the isopycnal heat flux accounts for less than 10 % of the total heat flux (Mercier et al., 2013). The different behavior between T_{cant} and heat fluxes across the OVIDE section is due to the differences in the horizontal gradient of Cant and temperature: Cant markedly decreases eastward due to the age of the water masses; meanwhile the temperature presents a subtle increase (see Fig. 2). As a result, high positive anomalies of Cant are found in the Irminger Sea, while the temperature anomalies are close to 0 °C. Therefore, the isopycnal contribution is more important in the T_{cant} than in the heat flux.

To go further in the analysis of the isopycnal transport of Cant in the Irminger Sea, we found that the overflow waters (DSOW and ISOW) and intermediate and surface waters are mainly responsible for the southward transport (Fig. 4d). The fact that intermediate and surface waters of the Irminger Sea have a high contribution to $T_{\text{cant}}^{\text{isop}}$ is because its high Cant concentration as compared to the waters with the same density range in the WEB and IAP as for example Mediterranean Water (see Fig. 2). The high Cant content in the intermediate waters of the Irminger Sea is likely due to the recent ventilation of these waters. Indeed, Våge et al. (2009) observed a 700 m-deep mixed layer in winter 2007–2008. In the case of the overflow waters, the relatively high Cant concentration is mainly due to the entrainment of Cant-rich thermocline water at the sills during the process of overflow (Sarafanov et al., 2010).

Once the waters mainly responsible for $T_{\text{cant}}^{\text{isop}}$ have been identified, the question is: why does the LSW, both upper and classical, yield a minor contribution to $T_{\text{cant}}^{\text{isop}}$ (see Fig. 4)? The answer is likely related to changes in the formation rate of these water masses and their spreading all along the OVIDE section. On the one hand, during the first half of the 90s, cLSW was abundantly formed in the Labrador Sea (Rhein et al., 2002), so it was enriched in Cant. In the mid-90s there was a shut-down in the formation of this water mass that was compensated by an enhanced production of uLSW in the Labrador Sea and possibly in the Irminger Sea (Yashayaev et al., 2007; Kieke et al., 2007; Rhein et al., 2011). Thenceforth, cLSW was exported to the Irminger Sea and northeast Atlantic, taking between 6 months (Sy et al., 1997) to 2 years (Straneo et al., 2003) to reach the Irminger Sea and 3–6 years to get to the Mid-Atlantic Ridge (Kieke et al., 2009). Because of this spreading, cLSW was homogenized all along the OVIDE section, resulting in small Cant anomalies. On the other hand, the evolution of $T_{\text{cant}}^{\text{isop}}$ in the uLSW density range during the period 1997–2010 displays more temporal variability (not shown), probably due to the intermittent ventilation of this water mass over the 2000s and to the advection timescales that are comparable to those of the cLSW. However, the average of $T_{\text{cant}}^{\text{isop}}$ in the density range of uLSW for the 1997–2010 period is close to zero; this is why we identify a minor contribution of uLSW to $T_{\text{cant}}^{\text{isop}}$, and a more detailed analysis of its variability is out of the scope of this study.

The decomposition of T_{cant} also shows that the overturning component ($T_{\text{cant}}^{\text{diap}}$) is the major contribution to T_{cant}, whose mean value over the period 1997–2010 is $400 \pm 29\,\text{kmol}\,\text{s}^{-1}$. Moreover, as in the case of heat flux, it drives the variability of T_{cant}. $T_{\text{cant}}^{\text{diap}}$ is related to the MOC_σ that transports warm and enriched Cant waters northward in its upper limb and denser, colder and poorer in Cant waters southward in its lower limb. The estimator T_{cant}° is a schematic representation of this mechanism and indeed we found a good correlation between T_{cant}° and $T_{\text{cant}}^{\text{diap}}$. It also offers a simple proxy for testing numerical models. However, we are aware that T_{cant}° does not represent all the processes involved in the transport of Cant in the SPNA.

It is well known that the MOC_σ presents a high seasonal variability. For example, Mercier et al. (2013) showed that it has a seasonal amplitude of 4.3 Sv. The data analyzed in this work were measured during summer months. Mercier et al. (2013) show that the MOC_σ at the OVIDE section presents its yearly minimum in summer, but their results also show that the interannual variability of the MOC_σ can be reliably represented by summer data. Therefore, we expect that the interannual variability of T_{cant} will be well captured by our study, although the magnitudes given in the present work are likely to be weaker than the annual means.

To get an order of magnitude of the relative importance at long timescales of the Cant content and the circulation on T_{cant} across the SPNA, we use T°_{cant}. On the one hand, Cant is increasing faster in the upper limb of the MOC_{σ} than in the lower limb, showing trends of $0.63 \pm 0.27\,\mu mol\,kg^{-1}\,yr^{-1}$ and $0.20 \pm 0.25\,\mu mol\,kg^{-1}\,yr^{-1}$, respectively, during the period 1997–2010. It means that, in the SPNA, there is more Cant being imported in the upper limb than being exported in the lower limb, resulting in an accumulation of Cant in the SPNA, in agreement with Sabine et al. (2004) and Pérez et al. (2010). The minor increase in Cant in the lower limb is due to the dilution of the convected and overflow waters rich in Cant with the deep waters poor in Cant. We expect that the Cant concentration in both limbs will be linked to the MOC_{σ} variability, although we do not know at which timescale. Indeed, it depends on the advection of water from the subtropical areas in the upper limb, and on the processes of deep and intermediate water formation in the lower limb. However, it is striking that ΔCant keeps increasing independently of the MOC_{σ} variability at a mean rate of $0.43 \pm 0.10\,\mu mol\,kg^{-1}\,yr^{-1}$ (see the pink line in Fig. 6a). This increasing rate is going to cause an augmentation in T_{cant} across the OVIDE section, and consequently, an increase in the storage rate in the SPNA. On the other hand, models have predicted a slow-down of 25 % of the MOC_{σ} at the end of the present century (IPCC, 2007) independently of the interannual to decadal variability observed by Mercier et al. (2013). Taking into account the predicted slow-down of the MOC_{σ} and the positive trend of ΔCant computed in this work, T°_{cant} would increase at a rate of $4.3 \pm 0.1\,kmol\,s^{-1}\,yr^{-1}$ during the 21st century. It means an increase of $430\,kmol\,s^{-1}$ of T_{cant} in 100 years, despite the predicted slow-down of the MOC_{σ}. To conclude, the faster increase in Cant in the upper limb than in the lower limb will cause an augmentation of the northward T_{cant} across the SPNA at long timescales. Nevertheless, at the timescale analyzed in this work (1997–2010), the interannual variability of the MOC_{σ} blurs the long-term increase in T_{cant} caused by the ΔCant increase. Furthermore, this result is quite speculative since (i) we suppose that the trend in ΔCant will remain constant and (ii) we rely on the models for the decrease in the MOC_{σ}. However, it gives an interesting order of magnitude.

We suspect that the long-term increase in T_{cant} would cause an increase in the storage rate of Cant in the SPNA. Pérez et al. (2013) observed a decrease in the storage rate of Cant in the SPNA between 1997 (high MOC_{σ}) and 2002–2006 (low MOC_{σ}). They reported a change in the storage rate from $0.083 \pm 0.008\,Gt\,C\,yr^{-1}$ to $0.026 \pm 0.004\,Gt\,C\,yr^{-1}$ between both periods. However, because of the short time span, the ΔCant increase was too small to compensate for the large intra-decadal decrease in the MOC_{σ} that caused the decrease in the T_{cant} across the OVIDE section and consequently the decrease in the Cant storage rate reported by Pérez et al. (2013). Calculating the storage rate for 1997–2010 is the subject of a future work.

To sum up, although the isopycnal transport has a considerable contribution to T_{cant} across the OVIDE section, the major contribution to T_{cant} is the diapycnal component, which is also the main driver of its variability. In both components of the transport, the Cant concentration plays an important role: the horizontal gradient of Cant across the section is responsible for the southward transport of Cant by the isopycnal component, while the Cant-laden waters flowing northward are responsible for the large positive values of the diapycnal component. Finally, we have shown that the variability of the MOC_{σ} dominates the variability of T_{cant} at interannual to decadal scales, but that the Cant increase seems to control the T_{cant} change at longer timescales. Therefore, in spite of the predicted slow-down of the MOC_{σ} by 2100, an increase in the storage rate of Cant in the SPNA would be expected.

Acknowledgements. We are grateful to the captains, staff and researchers who contributed to the acquisition and processing of hydrographic data. The research leading to these results was supported through the EU FP7 CARBOCHANGE "Changes in carbon uptake and emissions by oceans in a changing climate" project, which received funding from the European Commission's Seventh Framework Programme under grant agreement no. 264879. For this work P. Zunino was supported by the former project and by the Ifremer postdoctoral program. M. I. Garcia-Ibáñez was supported by the Spanish Ministry of Economy and Competitiveness (BES-2011-045614) through the CATARINA project (CTM2010-17141) co-funded by the Fondo Europeo de Desarrollo Regional 2007-2012 (FEDER); this article is going to be part of her PhD that is attached to the framework of the "Marine Science, Technology and Management" (DO*MAR) doctoral program of the University of Vigo. P. Lherminier was supported by the French Institute for Marine Science (Ifremer), H. Mercier by the French National Center for Scientific Research (CNRS), and A. F. Rios and F. F. Pérez by the Consejo Superior de Investigaciones Científicas (CSIC). We also acknowledge the anonymous reviewers for their help in improving the manuscript.

Edited by: L. Bopp

The publication of this article is financed by CNRS-INSU.

References

Alvarez, M. F., Bryden, H. L., Pérez, F. F., Rios, A. F., and Roson, G.: Physical and biogeochemical fluxes and net budgets in the subpolar and temperate North Atlantic, J. Mar. Res., 60, 191–226, 2002.

Alvarez, M., Rios, A. F., Pérez, F. F., Bryden, H. L., and Roson, G.: Transports and budgets of total inorganic carbon in the Subpo-

lar and Temperate North Atlantic, Global Biogeochem. Cy., 17, 1002, doi:10.1029/2002GB001881, 2003.

Billant, A., Branellec, P., and Mercier, H.: Campagne OVIDE 2002: Rapport de données CTD-O2, Tech. Rep. DRO/DOPS/04-01, 2004.

Böning, C. W. and Herrmann, P.: Annual cycle of poleward heat transport in the ocean: results from high-resolution modeling of the north and equatorial Atlantic, J. Phys. Oceanogr., 24, 91–107, 1994.

Branellec, P. and Thierry, V.: Campagne OVIDE 2010: Rapport de données CTDO2, Tech. Rep. ODE/OPS/LPO/13-01, 2013.

Bryden, H. and Imawaki, S.: Ocean heat transport, in: Ocean Circulation and Climate, edited by: Siedler, G., Church, J., and Gould, J., Academic Press, 2001.

Clayton, T. D. and Byrne, R. H.: Calibration of m-cresol purple on the total hydrogen ion concentration scale and its application to CO_2-system characteristics in seawater, Deep-Sea Res. Pt. I, 40, 2115–2129, 1993.

Ganachaud, A. and Wunsch, C.: Large-Scale Ocean Heat and Freshwater Transports during the World Ocean Circulation Experiment, J. Climate, 16, 696–705, 2003.

Gourcuff, C., Lherminier, P., Mercier, H., and Le Traon, P. Y.: Altimetry combined with hydrography for ocean transport estimation, J. Atmos. Ocean. Tech., 28, 1324–1337, doi:10.1175/2011JTECHO818.1, 2011

Grist, J. P., Marsh, R., and Josey, S. A.: On the relationship between the North Atlantic meridional overturning circulation and the surface-forced overturning streamfunction, J. Climate, 22, 4989–5002, doi:10.1175/2009JCLI2574.1, 2009.

Gruber, N. et al.: Oceanic sources, sinks, and transport of atmospheric CO2, Global Biogeochem Cy, 23, GB1005 (2009).

Khatiwala, S., Tanhua, T., Mikaloff Fletcher, S., Gerber, M., Doney, S. C., Graven, H. D., Gruber, N., McKinley, G. A., Murata, A., Ríos, A. F., and Sabine, C. L.: Global ocean storage of anthropogenic carbon, Biogeosciences, 10, 2169–2191, doi:10.5194/bg-10-2169-2013, 2013.

Kieke, D., Rhein, M., Stramma, L., Smethie, W. M., Bullister, J. L., and LeBel, D. A.: Changes in the pool of Labrador Sea Water in the subpolar North Atlantic, Geophys. Res. Lett., 34, L06605, doi:10.1029/2006GL028959, 2007.

Kieke, D., Klein, B., Stramma, L., Rhein, M., and Koltermann, K. P.: Variability and propagation of Labrador Sea Water in the southern subpolar North Atlantic, Deep-Sea Res. Pt. I, 56, 1656–1674, 2009.

Lherminier, P., Mercier, H., Gourcuff, C., Alvarez, M., Bacon, S., and Kermabon, C.: Transports across the 2002 Greenland-Portugal Ovide section and comparison with 1997, J. Geophys. Res., 112, C07003, doi:10.1029/2006JC003716, 2007.

Lherminier, P., Mercier, H., Huck, T., Gourcuff, C., Perez, F. F., Morin, P., Sarafanov, A., and Falina, A.: The Atlantic Meridional Overturning Circulation and the subpolar gyre observed at the A25-OVIDE section in June 2002 and 2004, Deep-Sea Res. Pt. I, 57, 1374–1391, doi:10.1016/j.dsr.2010.07.009, 2010.

Lux, M., Mercier, H., and Arhan, M.: Interhemispheric exchanges of mass and heat in the Atlantic Ocean in January–March 1993, Deep-Sea Res. Pt. I, 48, 605–638, 2000.

Macdonald, A. M., Baringer, M. O., Wanninkhof, R., Lee, K., and Wallace, D. W. R.: A 1998–1992 comparison of inorganic carbon and its transport across 24.51° N in the Atlantic, Deep-Sea Res. Pt. II, 50, 3041–3064, 2003.

Meehl, G. A., Stocker, T. F., Collins, W. D., Friedlingstein, P., Gaye, A. T., Gregory, J. M., Kitoh, A., Knutti, R., Murphy, J. M., Noda, A., Raper, S. C. B., Watterson, I. G., Weaver, A. J., and Zhao, Z.-C.: Global Climate Projections, in: Climate Change 2007: The Physical Science Basis.Contribution of Working Group I to the Fourth Assessment Report of the Intergovernmental Panel on Climate Change, edited by: Solomon, S., Qin, D., Manning, M., Chen, Z., Marquis, M., Averyt, K. B., Tignor, M., and Miller, H. L., Cambridge University Press, Cambridge, United Kingdom and New York, NY, USA, 2007.

Mercier, H.: Determining the general circulation of the ocean: a non linear inverse problem, J. Geophys. Res., 91, 5103–5109, 1986.

Mercier, M., Lherminier, P., Sarafanov, A., Gaillard, F., Daniault, N., Desbruyères, D., Falina, A., Ferron, B., Gourcuff, C., Huck, T., and Thierry, V.: Variability of the meridional overturning circulation at the Greenland-Portugal OVIDE section from 1993 to 2010, Prog. Oceanogr., doi:10.1016/j.pocean.2013.11.001, 2013.

Mikaloff-Fletcher, S. E., Gruber, N., Jacobson, A. R., Doney, S. C., Dutkiewicz, S., Gerber, M., Follows, M., Joos, F., Lindsay, K., Menemenlis, D., Mouchet, A., Müller, S. A., and Sarmiento, J. L.: Inverse estimates of anthropogenic CO_2 uptake, transport, and storage by the ocean, Global Biogeochem. Cy., 20, GB2002, doi:10.1029/2005GB002530, 2006.

Mintrop, L., Pérez, F. F., Gonzalez-Davila, M., Santana-Casiano, M. J., and Kortzinger, A.: Alkalinity determination by potentiometry: Intercalibration using three different methods, Ciencias Marinas, 26, 23–37, 2000.

Pérez, F. F. and Fraga, F.: A precise and rapid analytical procedure for alkalinity determination, Mar. Chem., 21, 169–182, 1987.

Pérez, F. F., Vázquez-Rodríguez, M., Mercier, H., Velo, A., Lherminier, P., and Ríos, A. F.: Trends of anthropogenic CO_2 storage in North Atlantic water Masses, Biogeosciences, 7, 1789–1807, doi:10.5194/bg-7-1789-2010, 2010.

Pérez, F. F., Mercier, H., Vázquez-Rodríguez, M., Lherminier, P., Velo, A., Pardo, P. C., Rosón, G., and Ríos, A. F.: Atlantic Ocean CO_2 uptake reduced by weakening of the meridional overturning circulation, Nat. Geosci., 6, 146–152, doi:10.1038/NGEO1680, 2013.

Rhein, M., Fischer, J., Smethie Jr., W. M., Smythe-Wright, D., Weiss, R. F., Mertens, C., Min, D.-H., Fleischmann, U., and Putzka, A.: Labrador Sea Water: pathways, CFC-inventory and formation rates, J. Phys. Oceanogr., 32, 648–665, 2002.

Rhein, M., Kieke, D., and Steinfeldt, R.: Ventilation of Upper Labrador Sea Water, 2003–2005, Geophys. Res. Lett., 34, L06603, doi:10.1029/2006GL028540, 2007.

Roson, G., Rios, A. F., Lavin, A., Bryden, H. L., and Pérez, F. F.: Carbon distribution, fluxes and budgets in the subtropical North Atlantic, J. Geophys. Res., 108, 3144, doi:10.1029/1999JC000047, 2003.

Sabine, C. L., Feely, R. A., Gruber, N., Key, R. M., Lee, K., Bullister, J. L., Wanninkhof, R., Wong, C. S., Wallace, D. W. R., Tilbrook, B., Millero, F. J., Peng, T.-H., Kozyr, A., Ono, T., and Rios, A. F.: The oceanic sink for anthropogenic CO_2, Science, 305, 367–371, 2004.

Sarafanov, A., Mercier, H., Falina, A., Sokov, A., and Lherminier, P.: Cessation and partial reversal of deep water freshening in the

northern North Atlantic: observation-based estimates and attribution, Tellus A, 62, 80–90, 2010.

Steinfeldt, R., Rhein, M., Bullister, J. L., and Tanhua, T: Inventory changes in anthropogenic carbon from 1997–2003 in the Atlantic Ocean between 20° S and 65° N, Global Biogeochem. Cy., 23, GB3010, doi:10.1029/2008GB003311, 2009.

Straneo, F., Pickart, R. S., and Lavender, K.: Spreading of Labrador sea water: an advective-diffusive study based on Lagrangian data, Deep-Sea Res. Pt. I, 50, 701–719, doi:10.1016/S0967-0637(03)00057-8, 2003.

Sy, A., Rhein, M., Lazier, J. R. N., Koltermann, K. P., Meincke, J., Putzka, A., and Bersch, M.: Surprisingly rapid spreading of newly formed intermediate waters across the North Atlantic Ocean, Nature, 386, 675–679, 1997.

Tanhua, T., Biastoch, A., Körtzinger, A., Lüger, H., Böning, C., and Wallace, D. W. R.: Changes of anthropogenic CO_2 and CFC in the North Atlantic between 1981 and 2004, Global Biogeochem. Cy., 20, GB4017, doi:10.1029/2006GB002695, 2006.

Tjiputra, J. F., Assmann, K., and Heinze, C.: Anthropogenic carbon dynamics in the changing ocean, Ocean Sci., 6, 605–614, doi:10.5194/os-6-605-2010, 2010.

Treguier, A.-M., Gourcuff, C., Lherminier, P., Mercier, H., Barnier, B., Madec, G., Molines, J.-M., Penduff, T., Czeschel, L., and Böning, C. W.: Internal and forced variability along a section between Greenland and Portugal in the CLIPPER Atlantic model, Ocean Dynam., 56, 568–580, 2006

Våge, K., Pickart, R., Thierry, V., Reverdin, G., Lee, C., Petrie, B., Agnew, T., Wong, A., and Ribergaard, M. H.: Surprising return of deep convection to the subpolar North Atlantic Ocean in winter 2007–2008, Nat. Geosci., 2, 67–72, doi:10.1038/NGEO382, 2009.

Vázquez-Rodríguez, M., Padin, X. A., Ríos, A. F., Bellerby, R. G. J., and Pérez, F. F.: An upgraded carbon-based method to estimate the anthropogenic fraction of dissolved CO_2 in the Atlantic Ocean, Biogeosciences Discuss., 6, 4527–4571, doi:10.5194/bgd-6-4527-2009, 2009.

Velo, A., Pérez, F. F., Lin, X., Key, R. M., Tanhua, T., de la Paz, M., Olsen, A., van Heuven, S., Jutterström, S., and Ríos, A. F.: CARINA data synthesis project: pH data scale unification and cruise adjustments, Earth Syst. Sci. Data, 2, 133–155, doi:10.5194/essd-2-133-2010, 2010.

Yashayaev, I., van Aken, H. M., Holliday, N. P., and Bersch, M.: Transformation of the Labrador Sea Water in the subpolar North Atlantic, Geophys. Res. Lett., 34, L22605, doi:10.1029/2007GL031812, 2007

Yashayaev, I. and Loder, J. W.: Enhanced production of Labrador Sea Water in 2008, Geophys. Res. Lett., 36, L01606, doi:10.1029/2008GL036162, 2009.